Blood Vessel Maturation and Response to Vascular-Disrupting Therapy in Single Vascular Endothelial Growth Factor-A Isoform–Producing Tumors

Gillian M. Tozer,[1] Simon Akerman,[1] Neil A. Cross,[1] Paul R. Barber,[2] Meit A. Björndahl,[1] Olga Greco,[1] Sheila Harris,[1] Sally A. Hill,[2] Davina J. Honess,[2] Christopher R. Ireson,[2] Katie L. Pettyjohn,[1] Vivien E. Prise,[2] Constantino C. Reyes-Aldasoro,[1] Christiana Ruhrberg,[3] David T. Shima,[3] and Chryso Kanthou[1]

[1]Cancer Research UK Tumour Microcirculation Group, Academic Unit of Surgical Oncology, School of Medicine and Biomedical Sciences, University of Sheffield, Sheffield, United Kingdom; [2]Gray Cancer Institute, Mount Vernon Hospital, Northwood, Middlesex, United Kingdom; and [3]Institute of Ophthalmology, University College London, London, United Kingdom

Abstract

Tubulin-binding vascular-disrupting agents (VDA) are currently in clinical trials for cancer therapy but the factors that influence tumor susceptibility to these agents are poorly understood. We evaluated the consequences of modifying tumor vascular morphology and function on vascular and therapeutic response to combretastatin-A4 3-*O*-phosphate (CA-4-P), which was chosen as a model VDA. Mouse fibrosarcoma cell lines that are capable of expressing all vascular endothelial growth factor (VEGF) isoforms (control) or only single isoforms of VEGF (VEGF120, VEGF164, or VEGF188) were developed under endogenous VEGF promoter control. Once tumors were established, VEGF isoform expression did not affect growth or blood flow rate. However, VEGF188 was uniquely associated with tumor vascular maturity, resistance to hemorrhage, and resistance to CA-4-P. Pericyte staining was much greater in VEGF188 and control tumors than in VEGF120 and VEGF164 tumors. Vascular volume was highest in VEGF120 and control tumors (CD31 staining) but total vascular length was highest in VEGF188 tumors, reflecting very narrow vessels forming complex vascular networks. I.v. administered 40 kDa FITC-dextran leaked slowly from the vasculature of VEGF188 tumors compared with VEGF120 tumors. Intravital microscopy measurements of vascular length and RBC velocity showed that CA-4-P produced significantly more vascular damage in VEGF120 and VEGF164 tumors than in VEGF188 and control tumors. Importantly, this translated into a similar differential in therapeutic response, as determined by tumor growth delay. Results imply differences in signaling pathways between VEGF isoforms and suggest that VEGF isoforms might be useful in vascular-disrupting cancer therapy to predict tumor susceptibility to VDAs. [Cancer Res 2008;68(7):2301–11]

Introduction

Disodium combretastatin-A4 3-*O*-phosphate (CA-4-P) is the lead compound of a group of tubulin-binding agents that act as vascular-disrupting agents (VDA) in solid tumors (1, 2). CA-4-P is active in human cancers (3) and is currently in phase II clinical trials in combination with conventional treatments (4).[4] VDAs cause a catastrophic collapse of blood flow to solid tumors and thus form a conceptually distinct group from the antiangiogenic agents (5).

Despite the progress of VDAs to clinical trials, and some evidence for improved patient survival upon adding VDA treatment to conventional chemotherapy (6), the reasons for the susceptibility of the tumor vasculature to VDAs remain unclear. Tumor blood vessels are generally considered to be immature. Thus, genetic modification of tumor cells to modulate expression of key molecules involved in vascular maturation provides a potential route for investigating the factors that influence the response of the tumor vasculature to VDAs.

Vascular endothelial growth factor A (VEGF-A or simply VEGF) is a key stimulator of tumorigenic angiogenesis (7) and acts as a mitogen, chemoattractant, survival factor, vasodilator, and permeability factor (8). Human and mouse VEGF mRNA is transcribed from eight exons and alternatively spliced to give rise to a number of isoforms of the protein product (9), the most prevalent consisting of 121, 165, and 189 amino acids in the human and 120, 164, and 188 in the mouse (Fig. 1*A*). VEGF120/121 lacks the heparin-binding site and is readily diffusible, whereas VEGF188/189 is tightly bound to proteoglycans in the extracellular matrix or on the cell surface and VEGF164/165 has intermediate properties. These isoforms are found in most normal tissues and have affinity for the VEGF receptors, FLT1 (VEGFR1) and KDR (VEGFR2; refs. 10, 11). VEGF121 and VEGF165 are the most prevalent forms in human cancers (12, 13).

Using Cre/Lox technology, mice expressing only single isoforms of VEGF, known as $Vegfa^{120/120}$, $Vegfa^{164/164}$, and $Vegfa^{188/188}$ mice, have been developed (14, 15). Their analysis revealed different roles for the individual VEGF isoforms in vascular growth and patterning during development. In particular, VEGF164 was sufficient for developmental angiogenesis and neonatal growth, and VEGF120 supported endothelial cell proliferation and vasculogenesis; however, angiogenic vessel branching was impaired and vessels

Note: Supplementary data for this article are available at Cancer Research Online (http://cancerres.aacrjournals.org/).

G.M. Tozer and S. Akerman contributed equally to this work.

Requests for reprints: Gillian M. Tozer, Cancer Research UK Tumour Microcirculation Group, Academic Unit of Surgical Oncology, K Floor, School of Medicine and Biomedical Sciences, University of Sheffield, Beech Hill Road, S10 2JF Sheffield, United Kingdom. Phone: 44-114271-2423; Fax: 44-114271-3314; E-mail: g.tozer@sheffield.ac.uk.

doi:10.1158/0008-5472.CAN-07-2011

[4] http://www.oxigene.com/

were hemorrhagic (16). VEGF188 was essential for the formation of a normal cardiovasculature in 50% of mice (14, 15).

In the current study, we used the single VEGF isoform-expressing mice and the counterpart wild-type mice to develop mouse fibrosarcoma cell lines from embryo fibroblasts. We reasoned that the different VEGF isoforms would give rise to tumors with very different vascular characteristics that could be used to investigate susceptibility to CA-4-P. The method of producing the tumor lines was substantially different from previous studies in which overexpression of individual VEGF isoforms was used (13, 17), ensuring that *VEGF* gene transcription was under the control of the endogenous VEGF promoter and thus susceptible to environmental control. We gained new insights into the differential effects of VEGF isoforms in tumors by using intravital microscopy and tumor uptake of i.v. administered markers to measure functional vascular end points, in addition to measuring vascular morphology and tumor growth, with and without CA-4-P.

Materials and Methods

Animal experiments were conducted in accordance with the United Kingdom Animals (Scientific Procedures) Act 1986 and with local ethical approval. CA-4-P was kindly provided by Professor G.R. Pettit (Arizona State University, Tempe, AZ).

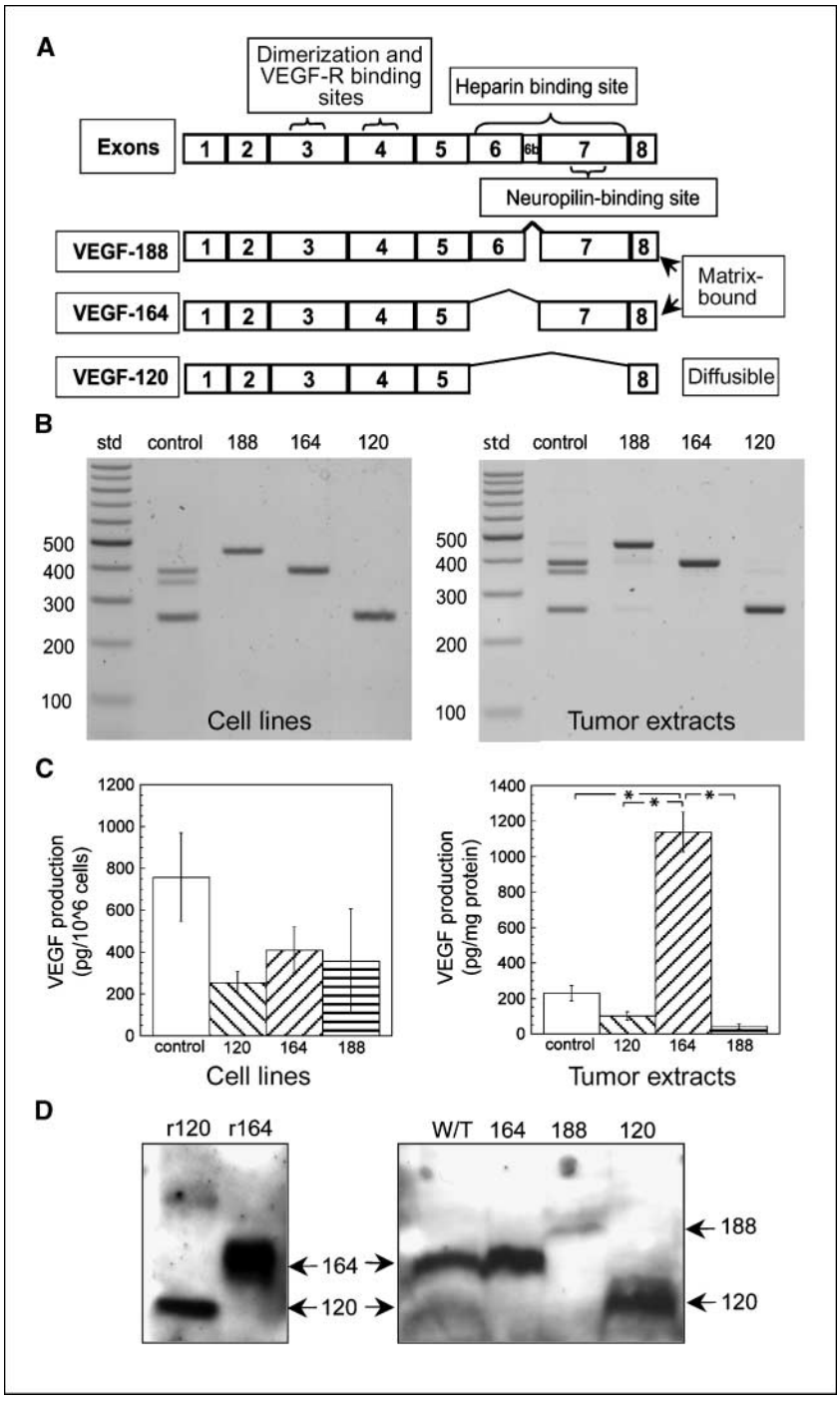

Figure 1. VEGF isoform expression. *A,* exon structure of murine VEGF isoforms. *B,* VEGF isoform–specific reverse transcription-PCR of cDNA extracted from control and single VEGF isoform–expressing tumor cell lines grown *in vitro* and solid tumor extracts from all four tumor types grown subcutaneously in SCID mice. Although bands corresponding to VEGF188, VEGF164, and VEGF120 are evident in control cell lines (*B*), only the relevant isoform is seen in each isoform-specific line. Alternative isoforms are just visible in each isoform-specific line when grown *in vivo* (*B*). Standards of known sizes were run in parallel (number of base pairs shown in the vertical bar). *C,* total VEGF protein level in conditioned medium from the different cell lines in culture and from tumor extracts, measured by ELISA. *Columns,* mean for five repeat cell culture experiments and for tumors ($n = 5$) in each group for tumor extracts; *bars,* SE. ANOVA showed no significant differences between groups in the cell culture experiments. *, $P < 0.05$, significant differences between groups for extracts of solid tumors (ANOVA followed by Tukey-Kramer HSD test). *D,* cell-conditioned media were concentrated 50-fold and analyzed by Western blotting using a VEGF antibody that recognizes all isoforms of VEGF-A. Mouse recombinant VEGF120 (*r120*) and VEGF164 (*r164*) migrated similarly to the medium conditioned by the single isoform–expressing tumor cells.

Tumor cell lines. Primary mouse embryo fibroblasts expressing single isoforms of VEGF (120, 164, or 188) only or all isoforms (Fig. 1*A*) were isolated from 13.5 dpc embryos produced by heterozygous breeding pairs of single VEGF isoform-expressing mice on a Swiss background. Fibroblast cultures were genotyped, as described (18), to identify wild-type samples and those homozygous for the *Vegfa*^{120}, *Vegfa*^{164}, or *Vegfa*^{188} allele. Fibroblasts were immortalized and oncogenically transformed by retroviral transduction with SV40 and HRAS (*h*-ras; refs. 19, 20). The resulting fibrosarcoma cell lines were maintained in high glucose DMEM (Invitrogen) medium containing L-glutamine, FCS, and the antibiotics G-418 and puromycin.

Apoptosis. Apoptotic cell death in response to CA-4-P was evaluated using the cell death detection ELISA^{plus} kit (Roche Diagnostics), as previously described (21). Cells were plated at 10^4 cells/well in 24-well plates, allowed to adhere for 24 h and then exposed to CA-4-P overnight before analysis.

Subcutaneous tumor transplantation. Fibrosarcoma cells expressing only VEGF120, VEGF164, or VEGF188 tumor cells or all three isoforms (control tumor cells) were injected s.c. (1×10^6 cells in 0.05 mL) into the rear dorsum of female severe combined immunodeficiency (SCID) mice (8–12 weeks old, 20–25 g).

VEGF-A mRNA and protein analysis. Excised tumors (6–8 mm diameter) were collected into RNAlater (Ambion). RNA and protein were isolated from tumor samples using the Mirvana PARIS kit (Ambion) and from cell lines in culture using the Cells-to-cDNA11 kit, according to the manufacturer's instructions. VEGF isoforms were amplified using the following PCR primers (forward, 5′CAGGCTGCTGTAACGATGAA3′; and reverse, 5′CTTTCCGGTGAGAGGTCTGG3′). Approximately 20% of each PCR reaction, together with appropriate controls, was then run on 2% agarose gels containing 1 μg/mL of ethidium bromide and products visualized under UV illumination.

For quantification of VEGF protein in culture supernatants, 2×10^6 cells were plated in T-175 flasks, and at 24 h, the medium was replaced with 20 mL of fresh medium. Cells were incubated for a further 48 h and then treated with 0.3 mmol/L of suramin for 3 h to release surface matrix-bound VEGF where medium was collected. VEGF was quantified in the cell medium and tumor extracts using the Quantikine Immunoassay mouse VEGF ELISA kit (R&D systems), according to the manufacturer's instructions.

An antibody recognizing all VEGF-A isoforms (p20, Santa Cruz Biotechnology) was used for Western blotting analysis. Cells were plated as above, but at 24 h, the medium was replaced with medium without serum. Conditioned media was collected 48 h later and concentrated 50-fold (Amicon). Equal amounts of proteins were separated on NuPAGE Novex gels (Invitrogen) and transferred to nitrocellulose membranes. Immunoreactive bands were detected by enhanced chemiluminescence.

Subcutaneous tumor growth. Subcutaneous tumors were measured using calipers and tumor volume (V) was calculated from $V = 0.52 \times d1 \times d2 \times d3$, where $d1$, $d2$, and $d3$ are the three orthogonal tumor diameters. Untreated tumor growth curves were fitted to "Gompertz" curves [$V = \exp(a - [b \times (\exp[-c \times (t - d)])])$], where *a, b, c*, and *d* are fitted variables, and t is time after transplant.

Tumors were treated when they reached 5 to 6 mm in diameter. CA-4-P (50 mg/kg i.p., 10 mL/kg in saline) or saline alone, was given once a day for 10 days, with a 2-day gap between the fifth and sixth doses.

Tumor histology and immunohistochemistry. Subcutaneous tumors (6–8 mm diameter) were formalin- or zinc-fixed, paraffin-embedded, and stained to identify endothelial cells (rat anti-mouse CD31 monoclonal antibody; BD PharMingen, Int.) and pericytes [mouse anti-mouse α-smooth muscle actin (α-sma) monoclonal antibody, Sigma-Aldrich; or rabbit anti-mouse desmin polyclonal antibody, Abcam; or rabbit anti-mouse angiopoietin-1 (ANG1) polyclonal antibody, Chemicon]. Antibody binding was visualized using 3,3′-diaminobenzidine (DakoCytomation) and signal amplification was achieved via the avidin-biotin complex/horseradish peroxidase system (CD31, α-sma, ANG1) or the EnVision system (desmin). Sections were counterstained with hematoxylin.

Mounted sections stained for CD31 and α-sma were quantified according to a random points scoring system (22). One hundred and twenty high-power regions of interest were counted per tumor to give vascular volume as a percentage of tumor volume for CD31 staining. The percentage of necrosis was measured from H&E sections by the same method or by delineation of necrotic regions in MATLAB (The Mathworks, Inc.). Desmin and ANG1 staining were assessed qualitatively.

Double staining immunofluorescence employed the CD31 monoclonal antibody described above and a FITC-conjugated monoclonal anti-mouse α-sma antibody (Sigma-Aldrich). Sections were incubated with a goat anti-rat Alexa-555 Red (Invitrogen) antibody. Sections were mounted in 4′,6-diamidino-2-phenylindole Vectashield (Vector Laboratories).

Window chamber surgery and tumor implantation. SCID mice (12–16 weeks old, 28–32 g) were anesthetized using fentanyl-fluanisone and midazolam i.p., as described previously (23). Briefly, an aluminum window chamber (total weight, ~2 g), holding two parallel glass windows, was implanted into a dorsal skin flap. A tumor fragment (~0.5 mm in diameter) from a donor animal was implanted onto the exposed panniculus muscle before closing the chamber, allowing a depth of ~200 μm for tumor growth. Animals were given a s.c. injection of dextrose saline (1 mL) and an i.p. injection of buprenorphine (0.1 mL, Vetergesic) to aid recovery and then kept in a warm room (28–30°C), until the day of the experiment.

Intravital microscopy. Donor RBC, acquired via cardiac puncture from donor mice were labeled with the fluorescent membrane dye, DiI (Invitrogen), for the measurement of RBC velocity in the tumor vasculature, as described previously (24–26). Tumors, at 3 to 5 mm in diameter, were used for treatment ~6 to 10 days after surgery.

Treated animals received either CA-4-P (30 mg/kg i.v. at a concentration of 3 mg/mL in 0.9% NaCl) or the same volume of 0.9% NaCl. Transmitted light images and video sequences (25 frames/s) were captured at various magnifications and time points up to 24 h after treatment. For the assessment of tumor vascularization in untreated tumors, imaging was performed once per day for several days after tumor transplantation.

Average vessel length, total vascular length, and fractal dimensions were acquired from transmitted light images using in-house–developed software, as described previously (23, 27). A single vessel was defined as a vascular length with no visible branches. RBC velocities were calculated from ×20 objective video sequences, using epifluorescence illumination, as described previously (26).

Macromolecular vascular leakage. FITC-labeled dextran (FITC-dextran; 40 kDa, 0.013 mol FITC/mol dextran; Sigma-Aldrich) was used as a macromolecular marker for determining tumor blood vessel barrier function. Following extensive washing to remove low-molecular weight contaminants, FITC-dextran (20 mg/mL) was made up in PBS and administered i.v. to awake, restrained mice at 0.05 mL per mouse. Multiphoton fluorescence microscopy, based on a modified Bio-Rad MRC 1024MP workstation, was used for imaging, as described previously (23). Images were captured every 4 min, at a working excitation wavelength of 890 nm. Emission wavelength was 530 to 540 nm. The three-dimensional data consisted of $512 \times 512 \times 11$ voxels each at a volume of $2.6 \times 2.6 \times 4.5$ μm^3.

Acquired images were processed, as described previously (28). Changes in image fluorescence intensity over time were used as an index of tumor vascular leakage of FITC-dextran. In addition, images from the first time point were analyzed for "contiguity" to provide a quantitative measure of vascular features in the different tumor lines. First, three-dimensional images were segmented into intravascular and extravascular classes, based on image intensities, as described previously (28). Then, each voxel within the intravascular class was interrogated to determine the fraction of neighboring voxels that were designated as being in the same class (29). The average of this fraction, derived from analysis of all the intravascular voxels from a particular tumor image, was defined as the contiguity of that tumor's vasculature. A highly contiguous vasculature suggests blood vessels that are well connected, with large diameters and extending into a large fraction of the tumor volume (diffuse).

Statistics. Statistical analysis was carried out using JMP Statistics version 5.1 for the Apple Macintosh (SAS Institute, Inc.). The Student's t test for unpaired data was used to test for significant differences between two groups. ANOVA followed by the Tukey-Kramer honest significance difference (HSD) test was used to test for significant differences between more than two groups. Time courses of intravital microscopy and tumor

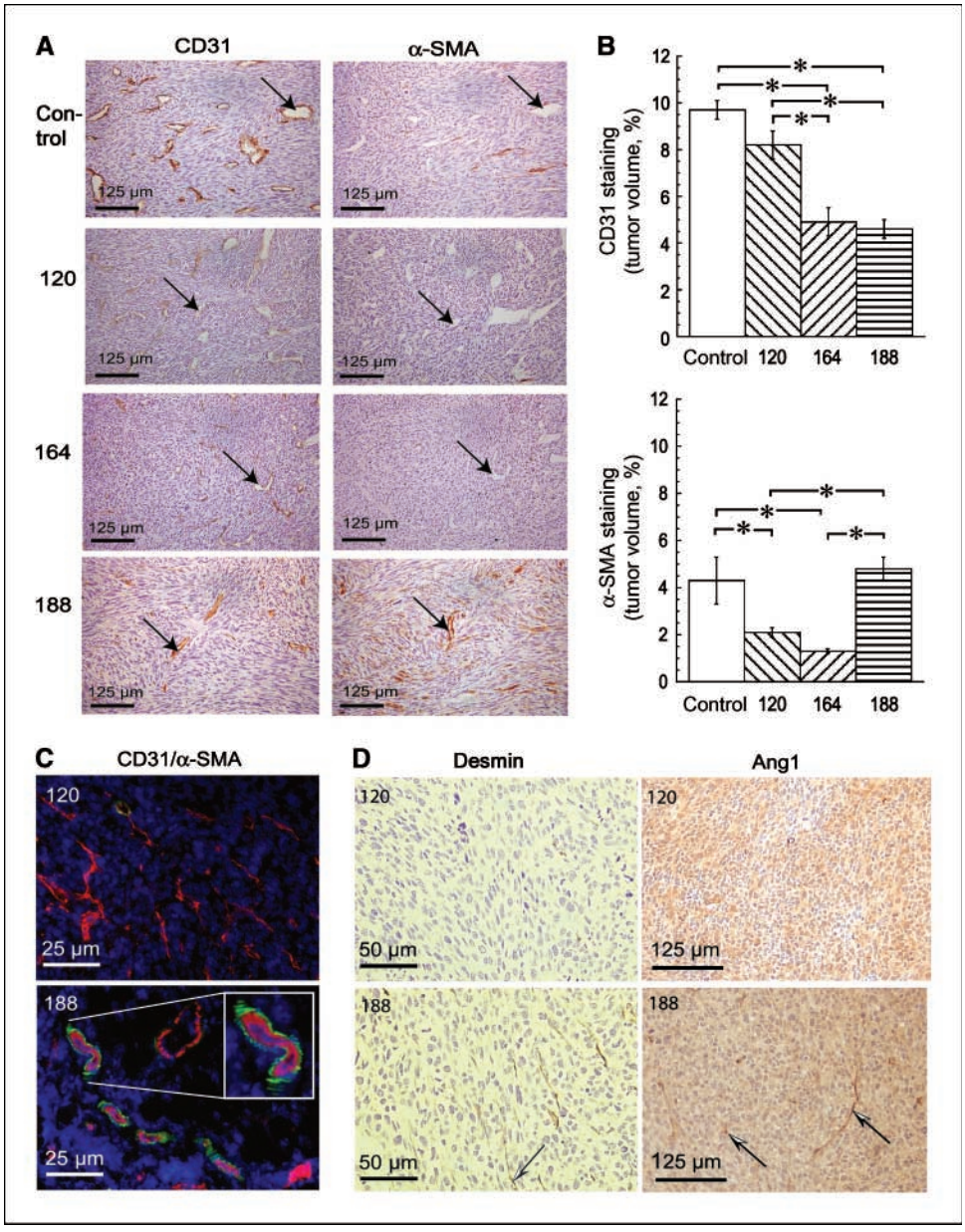

Figure 2. Immunohistochemical analysis of vascular wall maturity in tumors grown subcutaneously in SCID mice. *A,* near-adjacent sections from all four tumor types were stained for CD31 and α-sma (*brown*). *Arrows,* the same blood vessel in each pair of images. VEGF188-expressing and control tumors expressed more α-sma than the other tumor types, some but not all of which were associated with CD31-positive blood vessels. *B,* quantitative analysis of CD31 and α-sma staining for the whole group, stained as in *A. Columns,* mean for tumors in each group ($n = 8$); *bars,* SE. *, $P < 0.05$, significant differences between groups (ANOVA followed by Tukey-Kramer HSD test). *C,* double immunofluorescence staining for CD31 (*red*) and α-sma (*green*) with nuclei stained with 4′,6-diamidino-2-phenylindole (*blue*). *Inset,* the area indicated at higher magnification, illustrating the spiraling morphology of pericytes. *D,* desmin staining and Ang1 staining (*brown*) for VEGF120- and VEGF188-expressing tumors. *Arrows,* examples of vessels staining positively for desmin and Ang1.

growth data were fitted to a multivariate model (MANOVA) with repeated measures, and differences in responses of the different lines were tested for significance using an approximate F test. In all cases, differences between groups were described as significant if the probability corresponding to the appropriate statistic was <0.05.

Results

VEGF isoform expression. Fibrosarcoma cell lines expressing only single isoforms of VEGF were generated from primary mouse embryo fibroblasts isolated from isoform-specific mice. Figure 1*B* shows that the isoform-specific cell lines expressed the expected VEGF isoform transcripts, when grown *in vitro* or as solid tumors *in vivo*. Some faint bands corresponding to alternative VEGF isoforms were apparent for each of the isoform-specific tumor lines when grown *in vivo*. These most likely derive from infiltrating normal mouse cells, as we have observed moderate macrophage infiltration in all four tumor types (data not shown). Control tumor cell lines predominantly expressed the VEGF164 and VEGF120 mRNA (Fig. 1*B*). Sequencing of the lower band of the doublet that is apparent just below VEGF164 in control tumor cell lines revealed a mixed sequence, which corresponded to VEGF164 and VEGF120 (data not shown), suggesting that these two isoforms could form a heteroduplex under these experimental conditions (30).

Total VEGF-A protein production, measured by ELISA, in conditioned medium from the cells, was not significantly different across the lines, although there was a tendency for the highest production in control cells (Fig. 1*C*). VEGF levels in cell lysates were very low by comparison (data not shown). For tumors *in vivo*, total VEGF levels, measured by ELISA, were highest in the VEGF164 line (Fig. 1*C*), despite equivalent quantitative gene expression levels across the lines (see Supplementary Fig. S1). This confirms a previous report of high VEGF165 protein levels following transfection of MCF-7 tumor cells with VEGF121, VEGF165, or VEGF189 (31). Hypoxia, a

common feature of the tumor microenvironment, was reported to affect all isoforms of VEGF-A in a similar manner. However, repeated oxygen fluctuations have been reported to specifically increase VEGF164 in the retina (32) and this may be relevant to our results.

Western analysis confirmed that the cell lines produced significant quantities of the appropriate VEGF isoform, and no others, when cultured *in vitro*. However, protein expression of the VEGF164 isoform was predominant and VEGF188 expression was low and below detection limits in the control cell line (Fig. 1*D*).

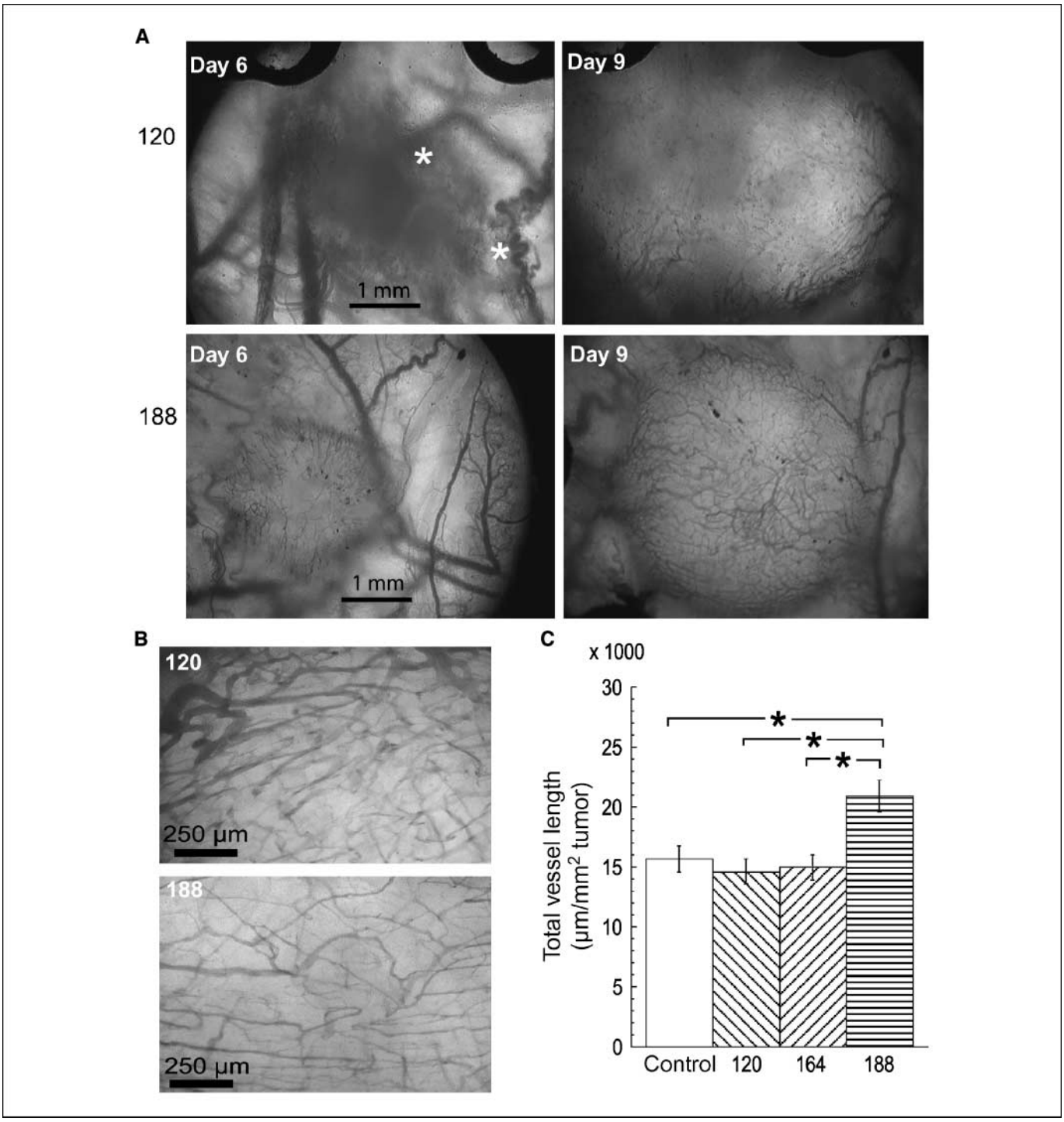

Figure 3. Vascular morphology of tumors growing in the dorsal skin flap window chambers in SCID mice. *A,* low-power (×2.5 objective) transmitted light images of tumors at 6 and 9 d after tumor transplantation. *, hemorrhage in the VEGF120-expressing tumor. Images show a well-vascularized center in the VEGF188-expressing tumor at day 9, as compared with the VEGF120-expressing tumor at the same time (see also Supplementary Fig. S2). *B,* high-power (×10 objective) images of VEGF120- and VEGF188-expressing tumors showing narrower vessels and a more regular arrangement of the vascular network in the VEGF188-expressing tumor. *C,* quantitative analysis of total vascular length in regions of interest such as those in *B*, for the whole group of tumors. *Columns,* mean for tumors in each group ($n = 6–9$); *bars,* SE. *, $P < 0.05$, significant differences between the groups. Total vascular length was significantly higher in VEGF188-expressing tumors than in the other tumor types (ANOVA followed by Tukey-Kramer HSD test).

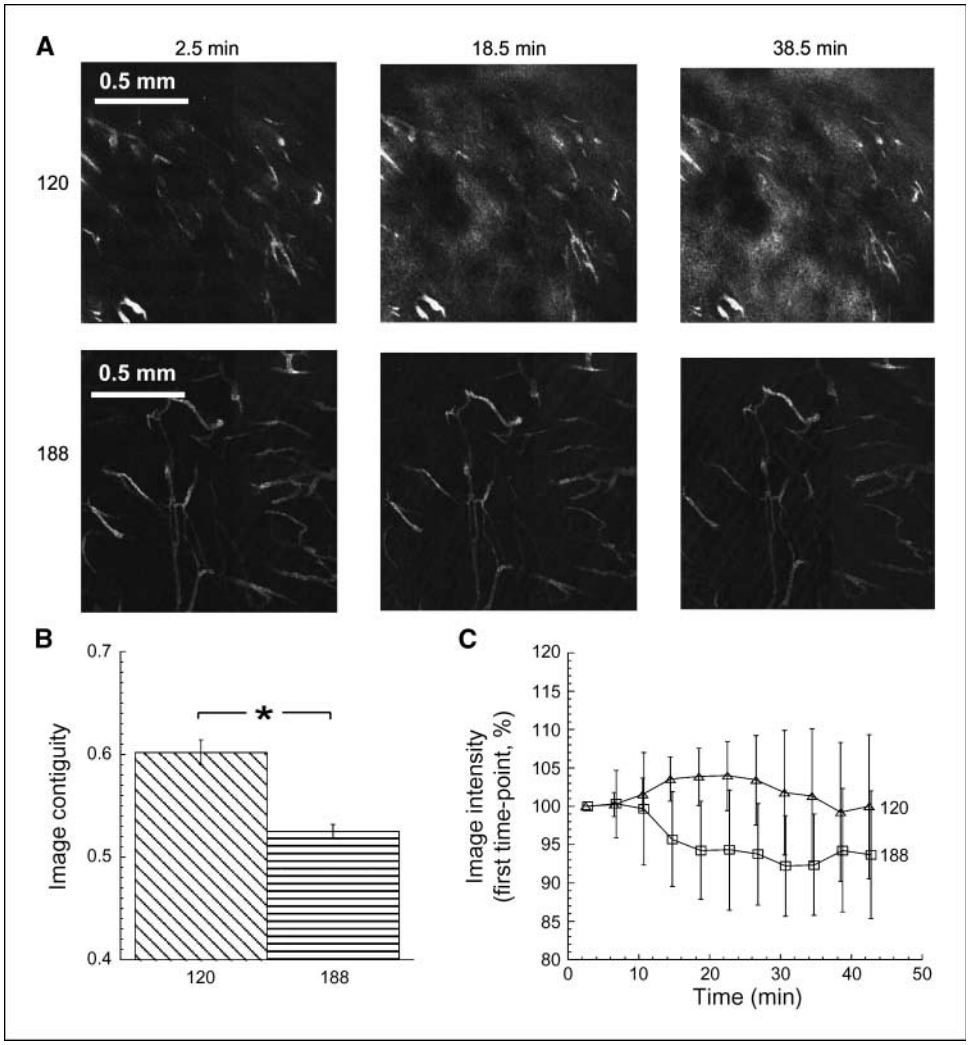

Figure 4. *In vivo* multiphoton fluorescence imaging of VEGF120- and VEGF188-expressing tumors growing in window chambers in SCID mice. *A,* maximum projection images from two tumors at different times (midpoint of the time frame for image acquisition) following i.v. injection of 40 kDa of FITC-dextran. Extensive leakage of FITC-dextran from the tumor vasculature into the interstitium could be seen with time in the VEGF120-expressing tumor but not in the VEGF188-expressing tumor. *B,* image contiguity (*columns,* mean; *bars,* SE) at the first time point after injection of FITC-dextran (2.5 min) for the whole tumor group (n = 5–7 tumors in each group). Contiguity was significantly higher in VEGF120 tumors than in VEGF188 tumors (*, P = 0.0005; Student's t test for unpaired data). *C,* the kinetics of FITC-dextran leakage for the whole tumor group. Intensities were averaged gray levels in whole three-dimensional images of each tumor, normalized to the first time point (mean for n = 5–7 tumors in each group; *bars,* 1 SE). The curves for the two groups were significantly different ($P < 0.05$, MANOVA with repeated measures).

Attempts to carry out Western analysis on solid tumor extracts were not successful, probably because levels were below the sensitivity limits of the assay.

Vascular morphology. Established subcutaneous tumors were examined for vascularity and maturity of their vessel walls using immunohistochemistry. CD31 staining in Fig. 2*A* shows that all tumor types were well-vascularized. However, α-sma staining shows that control and VEGF188-expressing tumors were better stabilized with pericytes than VEGF120- or VEGF164-expressing tumors. Although this staining was apparent in blood vessel walls, there was also substantial staining in a subset of extravascular cells. Quantification of staining (Fig. 2*B*) showed that control and VEGF120 tumors were the most vascular (CD31), whereas control and VEGF188 tumors had the most α-sma staining. These differences were statistically significant (see legend for details). Further investigations were carried out in the VEGF120-expressing (most diffusible) and the VEGF188-expressing (nondiffusible) tumors. Figure 2*C* shows double-staining for CD31 and α-sma, which confirmed the localization of α-sma–positive cells (pericytes) in the vasculature of VEGF188 tumors and very little staining in the VEGF120 tumors. The spiraling morphology of the α-sma staining in the VEGF188 tumor indicates close contact between pericytes and endothelial cells. Figure 2*D* shows that desmin- and ANG1-positive cells were also preferentially found in VEGF188 tumors rather than in VEGF120 tumors. The staining patterns were also highly suggestive of vascular localization. Taken together, these results indicate the association of VEGF120 with sustained expansion of the tumor vasculature, whereas VEGF188 is uniquely associated with maturation of the blood vessel wall.

Vascularization of single VEGF isoform–expressing tumors was further analyzed by intravital microscopy. Figure 3*A* and Supplementary Fig. S2 illustrate the vascularization of VEGF120- and VEGF188-expressing tumors at early and late phases of growth in the window chamber. Initial vascularization of the VEGF120-expressing tumors was typified by dilated preexisting normal blood vessels, which were prone to hemorrhage and indistinct tumor margins (Fig. 3*A*). In contrast, preexisting normal vessels were narrower in the VEGF188 implants, there was very little or no hemorrhage and the tumor margins were distinct. As tumors grew, hemorrhage within the VEGF120-expressing tumors tended to resolve but vascularization was often limited to the periphery of the tumor mass. In contrast, VEGF188-expressing tumors were vascularized throughout the tumor mass (Fig. 3*A*). Control and VEGF164-expressing tumors had intermediate properties.

Quantitative morphologic analysis of tumor blood vessels was carried out on two peri-peripheral regions of interest within each

tumor, using a ×10 objective, once the tumors became optimally vascularized. The vascular patterning in the VEGF188 tumors stood out from the others in that the blood vessels were arranged more regularly and individual vessels were uniformly narrow. Blood vessels in the other tumor types were irregular in width but generally wider and very chaotic in their arrangement. Typical regions of interest in a VEGF120- and VEGF188–expressing tumor are shown in Fig. 3*B*. Quantitative analysis revealed no significant difference between the tumor lines in terms of mean vascular lengths or fractal dimensions (data not shown). However, the total vascular length was higher in the VEGF188 tumors than in any of the other tumor types (Fig. 3*C*).

Vascular function. Leakage of i.v. injected 40 kDa fluorescent dextran was monitored in VEGF120 and VEGF188 tumors growing in window chambers, using multiphoton fluorescence microscopy (Fig. 4). Figure 4*A* shows typical images with diffuse vascularization and rapid leakage in a VEGF120 tumor compared with a VEGF188 tumor. Contiguity data for the whole group (Fig. 4*B*), is consistent with the diffuse nature of the vasculature in VEGF120 tumors, wider diameter vessels, and leakiness. Figure 4*C* shows the kinetics

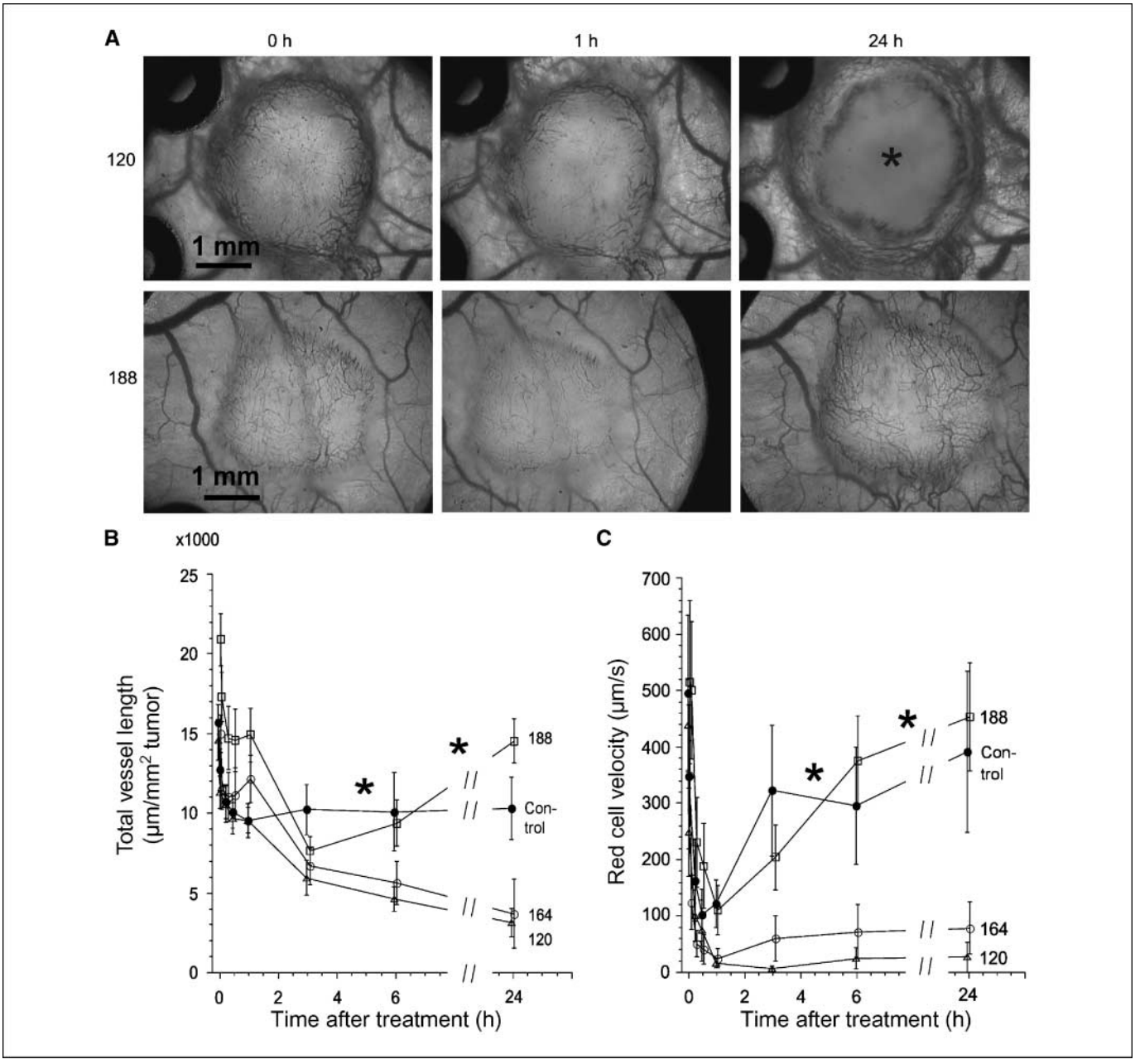

Figure 5. Response of the different tumor types growing in window chambers in SCID mice to a single dose of 30 mg/kg i.v. CA-4-P. *A,* typical low-power (×2.5 objective) images of VEGF120- and VEGF188-expressing tumors after CA-4-P treatment. There was a reduction in the visible vasculature at 1 h after treatment in both tumor types and extensive avascular regions in VEGF120- but not VEGF188-expressing tumors by 24 h (*). Supplementary Fig. S3 shows that the response of VEGF164 tumors was similar to VEGF120 tumors and the response of control tumors was similar to VEGF188 tumors. *B* and *C*, quantitative analysis of vascular length and red cell velocity for all tumor types. *Points,* mean for tumors in each group (n = 4–6); *bars,* SE. *, $P < 0.05$, curves for VEGF120- and VEGF164-expressing tumors were significantly different from those for VEGF188-expressing and control tumors over these regions (MANOVA with repeated measures).

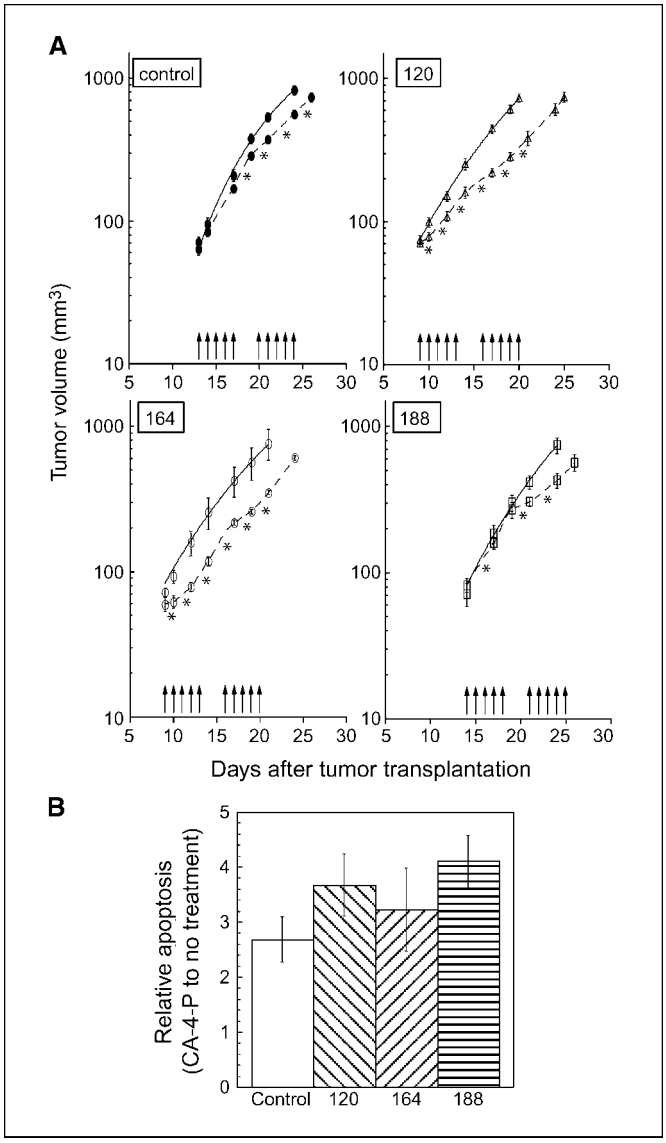

Figure 6. *A,* tumor volume growth curves for all tumor types growing subcutaneously in SCID mice ± CA-4-P treatment [10 fractions of 50 mg/kg of CA-4-P i.p. or equal volumes of saline, at times indicated (*arrows*)]. Untreated tumor growth curves (*solid lines*) were fitted to Gompertz curves, as described in the text. The lag phase in tumor growth was shorter for VEGF120 and VEGF164 tumors than for control and VEGF188 tumors. However, at 18 d, untreated tumor growth rate was 73.4 ± 7.8, 86.2 ± 8.0, 86.3 ± 18.3, 59.2 ± 5.4 mm^3/d for control, VEGF120-, VEGF164-, and VEGF188-expressing tumors, respectively. These differences were not significant ($P > 0.05$, ANOVA), which was consistent with similar blood flow rates in the four cell lines (see Supplementary Fig. S4). VEGF120- and VEGF164-expressing tumors responded better to CA-4-P treatment (*broken lines*) than VEGF188-expressing and control tumors. *Points,* mean for tumors in each group, representing combined data from two separate experiments ($n = 9–11$); *bars,* SE. *, $P < 0.05$, significant differences were obtained between untreated and treated curves over the regions indicated (MANOVA with repeated measures). *B,* apoptosis induced by CA-4-P (100 μmol/L) in single isoform–expressing tumor cells and control cells *in vitro*. Results are plotted as rates relative to those in untreated cells. *Columns,* mean for seven repeat experiments; *bars,* SE. There were no significant differences across the groups ($P > 0.05$, ANOVA).

of fluorescence intensity in tumors with time after injection of FITC-dextran. There was a significant difference between the VEGF120 and VEGF188 tumors, with average intensity decreasing with time in the VEGF188 tumors and maintained or increasing in VEGF120 tumors. This difference was consistent with more rapid leakage of FITC-dextran from the intravascular to extravascular space in the VEGF120 tumors, which maintained average image intensity in the face of vascular clearance of the marker.

Response to CA-4-P. Vascular response to CA-4-P was determined in tumors growing in window chambers. Figure 5*A* shows typical images from VEGF120- and VEGF188-expressing tumors at 0, 1, and 24 h following treatment with a moderate single dose of CA-4-P (30 mg/kg i.v.). Response in both tumor types was typified by a substantial loss of the visible vasculature, primarily at the tumor center, at 1 h after treatment. Subsequently, VEGF120-expressing tumors progressed to almost complete avascularity and opacity of the central tumor region at 24 h. The vascular morphology was substantially less affected in the VEGF188 tumors, with very little avascularity by 24 h (Fig. 5*A*).

Quantitation of the vascular damage in window chamber tumors following CA-4-P treatment is shown in Fig. 5*B* and *C* for all the tumor types. There is a clear distinction in response between the VEGF120 and VEGF164 tumors on the one hand, and the wild-type and VEGF188 tumors on the other, confirming the observations shown in Fig. 5*A* and Supplementary Fig. S3, which gives additional images from all tumor types. The distinction in response of the different tumor types was clearly apparent from both a morphologic end point (total vessel length; Fig. 5*B*) and a functional end point (red cell velocity; Fig. 5*C*).

In order to determine whether these differences in early vascular response to CA-4-P translated into differences in therapeutic response, a repeat dosing schedule of CA-4-P was administered to mice bearing subcutaneous tumors (Fig. 6*A*). VEGF120 and VEGF164 tumors were, again, the most sensitive. Interestingly, although the control and VEGF188 tumors seemed to be completely resistant to the effects of CA-4-P in the first week of treatment, there was some growth retardation during the second week. In a separate experiment, VEGF120-expressing tumors were significantly more necrotic than VEGF188-expressing tumors at 24 h after a single 100 mg/kg dose of CA-4-P (79.5 ± 9.3% versus 42.8 ± 9.3% of tumor volume, respectively, $P < 0.05$ for Student's t test). However, after five doses of 50 mg/kg CA-4-P, as in Fig. 6*A*, the necrosis levels in the two tumor types were very similar (34.3 ± 7.2% and 41.1 ± 9.2%, respectively), suggesting that the responsiveness of the 188 tumors in the second week was due to increased sensitivity of the vasculature. Vascular volume in viable regions of VEGF120-expressing tumors, as measured by CD31 staining, significantly increased from 7.2 ± 0.5% to 11.0 ± 0.6% of tumor volume after a week's treatment ($P < 0.05$ for Student's t test). A similar trend in the VEGF188-expressing tumors was only borderline significant. Figure 6*A* also shows that untreated VEGF120- and VEGF164-expressing tumors reached a measurable size ~4 days before the VEGF188 and control tumors, but then, all lines grew at the same rate, consistent with comparable blood flow rates (Supplementary Fig. S4). CA-4-P (100 μmol/L) increased apoptosis in all the cell lines growing *in vitro*, with no significant difference in induction rates between the different cell lines (Fig. 6*B*).

Discussion

We have shown that mouse fibrosarcoma cells, which express only single isoforms of VEGF, under the control of the endogenous VEGF promoter, produce tumors with very different vascularization patterns, vessel wall structure, and barrier function. The method used for production of the tumor lines ensured normal overall VEGF levels. Expression of VEGF188, even at very low levels,

was uniquely associated with extensive recruitment of vascular support cells (pericytes) and tumor resistance to the VDA CA-4-P. Overall, our results support the view that VEGF188 expression results in a different type of vascular bed, which renders the tumor vasculature less susceptible to CA-4-P.

Our data support previous findings that VEGF120/121 is associated with hemorrhage and vasodilation around tumors (33, 34). They are in agreement with Grunstein et al. (17) who found that VEGF120 and VEGF164 were associated with rapid initiation of fibrosarcoma growth. In contrast with our findings, Grunstein et al. found poor tumor growth associated with a fibrosarcoma cell line expressing only VEGF188. This may be due to high levels of VEGF188 in their overexpressing tumor line, leading to overvascularization of tumors. Indeed, Grunstein et al. found particularly poor vascular filling of contrast agent in their VEGF188-expressing tumors. In both studies, endogenous VEGF production from normal cells such as macrophages might be expected to contribute to vascular development. We found moderate macrophage invasion in all tumor types. However, our reverse transcription-PCR results showed that host-derived expression of VEGF isoforms was very low in all tumors and this was consistent with substantial differences in the vascular characteristics we observed. Quantitative differences in expression levels may explain why some authors have found that tumor cells transfected to overexpress VEGF188/189 are nontumorigenic (13), whereas others are tumorigenic (34–36). Interestingly, selective down-regulation of VEGF189 expression in a non–small cell lung cancer (35) and pancreatic cancer cell line (36) significantly reduced their xenotransplantability, suggesting that VEGF188/189 does play an important role in tumorigenesis.

We found striking differences in the maturation status of the vascular wall in the different VEGF isoform–producing tumors, which related to response to CA-4-P. In particular, the presence of VEGF188 resulted in tumor vascular recruitment of mural cells. This is consistent with the observations that mice selectively expressing VEGF188 recruit mural cells normally to the developing retinal venules and capillaries, whereas mice selectively expressing VEGF120 show major defects in mural cell recruitment (15). In addition, we showed that ANG1 was expressed in a subset of vessels in VEGF188 tumors and that barrier function in the VEGF188 tumors was more effective than in VEGF120 tumors, consistent with the observed structural differences. The processes involved in mural cell recruitment are complex and poorly understood but undoubtedly involve growth factors in addition to VEGF, such as platelet-derived growth factor B (PDGFB; ref. 37). Nevertheless, the current result clearly shows a key role for VEGF188 in mural cell recruitment in tumors that is associated with a functional effect. In addition, positive staining for α-sma was found in a subset of extravascular cells, presumably tumor cells or fibroblasts, of the VEGF188-expressing and control tumors but not in the VEGF120- or VEGF164-expressing tumors. This suggests a novel role for VEGF188/189 in pericyte differentiation.

Vascular network development was highly influenced by differential expression of VEGF isoforms, with VEGF120 being associated with a high vascular volume in established subcutaneous tumors and VEGF188 being associated with regular, narrow vessels and a high vascular length per tumor volume. In tumors growing in window chambers, which are subjected to high tissue pressure induced by the restraining glass, VEGF120 and VEGF164 were associated with a failure to effectively vascularize the center of tumors. This is likely to be due to the fragility of blood vessels, suggested by their lack of mural cells. Expression of VEGF164 was associated with a relatively low vascular volume (similar to VEGF188) but rapid initiation of tumor growth (similar to VEGF120). This suggests a highly proliferating phenotype for VEGF120- and VEGF164-expressing tumor cells, at the expense of vascular maturation. This is consistent with our recent *in vitro* data, showing higher proliferation rates for VEGF120- or VEGF164-expressing tumor cells than VEGF188-expressing or control cells (ref. 20; Supplementary Table S1). Any differences between the vasculature in VEGF120- and VEGF164-expressing tumors were subtle. However, the difference in vascular volume and the qualitative observation of less hemorrhage in the VEGF164 tumors does suggest some differences in their control of vascular maturation, an observation that warrants further investigation.

Several explanations for the different effects of individual VEGF isoforms on tumor vascular morphology and function can be envisaged. In the developing brain of $Vegfa^{188/188}$ mice, there is an increased extension of endothelial filopodia and vascular branch formation, compared with brains of $Vegfa^{120/120}$ mice (16), and this might also apply to tumor angiogenesis. There is also evidence for differential activation of VEGF receptors by the different isoforms. First, VEGF164/165 (and probably VEGF188/189) but not VEGF120/121, can bind to the accessory receptor, neuropilin-1 (NRP1; ref. 38). However, impaired signaling through the NRP-1 receptor could not account for all vascular branching defects in $Vegfa^{120/120}$ mouse embryos (16) and would not explain the significant differences between VEGF164- and VEGF188-expressing tumors. Heparan sulfate proteoglycans on the cell surface have also been implicated in modifying VEGF signaling, partly by controlling the distribution and bioavailability of secreted VEGF (39, 40). Other possibilities, which remain poorly understood, include the translocation of intracellular VEGF188/189 to the nucleus (31) and the cross-talk of VEGF signaling pathways with integrins (41).

In interpreting our data, we cannot discount the possibility that an adaptive response to the depletion of VEGF120 or VEGF164, resulting in increased expression of alternative vascular-related growth factors in the VEGF188-expressing cell line, could explain our results. Notwithstanding potential affinity issues of the VEGF antibody used in the ELISA kit for VEGF188, VEGF protein expression in the VEGF188 line *in vivo* seems to be relatively low (Fig. 1*C*), highlighting this possibility. However, real-time PCR data (Supplementary Fig. S1) did not reveal any alternative candidate genes for explaining our results. Transformation significantly lowered *VEGFR2, NRP1, TIE2, Ang2*, and *Hey2* gene expression across all the lines, but only Ang2 and PDGFB differed in their expression levels between the VEGF188-expressing tumor cells and the other cell types. Increased Ang2 and lowered PDGFB levels, as found in the VEGF188-expressing line, are unlikely explanations for the observed increase in pericyte recruitment of this line *in vivo* because Ang2 is normally associated with vascular immaturity and PDGFB is a well-known chemoattractant for pericytes. In addition, administration of VEGF receptor kinase inhibitors *in vitro* and *in vivo* and a pan-isoform neutralizing antibody for VEGF *in vitro*, equalized both tumor cell proliferation *in vitro* and vascular morphology *in vivo*, across the different cell lines, suggesting that baseline differences in these variables were VEGF-induced (Supplementary Fig. S5; Supplementary Table S1).

Differential expression of VEGF isoforms was clearly associated with outcome following treatment with the VDA, CA-4-P, both in terms of initial vascular response and tumor growth response to a repeated dosing schedule. A modest growth response, as observed

here even for the VEGF120-expressing tumors, is not unusual for VDAs and could mask significant cell-killing effects. This is thought to be due primarily to poor clearance of dead cells because of blood flow reduction (42). The presence of VEGF188, even at low levels in the control tumors, conferred resistance to treatment. Although speculative, it is possible that very tight association of VEGF188 with the cell surface minimizes the amount of protein necessary for a given outcome, as well as negatively feeding back on VEGF188 production. Necrosis data showed that VEGF188 tumors suffered vascular damage in the first week of treatment despite the lack of growth response. This may have been sufficient to sensitize the tumors to continued treatment. CD31 staining indicated an increase in vascularization of re-growing viable tumor regions after the first week of treatment, which could relate to homing of bone marrow–derived vascular progenitor cells following CA-4-P treatment, as previously reported (43). This increased vascularization may also relate to increased sensitivity to CA-4-P in the second week of treatment, although potential mechanisms require further investigation. Finally, the larger size of tumors at the start of treatment in the second week may have contributed to increased sensitivity (44).

Previously, we hypothesized that high vascular permeability and the immaturity of the vascular wall were major factors associated with the sensitivity of tumor vasculature to CA-4-P and similar agents (45, 46). The current results substantiate this hypothesis, and furthermore, suggest that VEGF188 expression is uniquely predictive of treatment outcome. Interestingly, several studies have suggested that VEGF189 expression in human cancers is associated with tumor progression and poor outcome from conventional treatments (47–50).

In conclusion, the main VEGF isoforms, under the control of the endogenous VEGF promoter, have very different effects on vascularization of fibrosarcomas in an animal model. In particular, VEGF188 and/or associated gene expression plays a crucial role in tumor vascular maturation and conferring resistance to the VDA, CA-4-P. Therefore, VEGF isoform expression may be useful for predicting tumor susceptibility to vascular-disrupting cancer therapy.

Acknowledgments

Received 5/30/2007; revised 12/3/2007; accepted 2/7/2008.

Grant support: Cancer Research UK Programme grant C1276/A3307.

The costs of publication of this article were defrayed in part by the payment of page charges. This article must therefore be hereby marked *advertisement* in accordance with 18 U.S.C. Section 1734 solely to indicate this fact.

We gratefully acknowledge Dr. Gabi Dachs, Dr. Andrew Steele, and Claudia Coralli for their roles in developing the tumor lines used in this study; Finuala Hylands, Ian Wilson, Frances Daley, and Matthew Fisher for their technical support; Professor Boris Vojnovic and Dr. Simon Ameer-Beg for their expertise and support with multiphoton-fluorescence microscopy; the Gray Cancer Institute, University of Sheffield and Cancer Research UK London Institute for care of the animals; and Professor Bob Pettit for supplying the CA-4-P.

References

1. Tozer GM, Kanthou C, Baguley BC. Disrupting tumour blood vessels. Nat Rev Cancer 2005;5:423–35.
2. Chaplin DJ, Horsman MR, Siemann DW. Current development status of small-molecule vascular disrupting agents. Curr Opin Investig Drugs 2006;7:522–8.
3. Galbraith SM, Maxwell RJ, Lodge MA, et al. Combretastatin A4 phosphate has tumor antivascular activity in rat and man as demonstrated by dynamic magnetic resonance imaging. J Clin Oncol 2003;21: 2831–42.
4. Young SL, Chaplin DJ. Combretastatin A4 phosphate: background and current clinical status. Expert Opin Investig Drugs 2004;13:1171–82.
5. Horsman MR, Siemann DW. Pathophysiologic effects of vascular-targeting agents and the implications for combination with conventional therapies. Cancer Res 2006;66:11520–39.
6. von Pawel J, Reck M, McKeage M. Update on survival in phase Ib/II study of DMXAA (AS1404) combined with carboplatin and paclitaxel in non-small cell lung cancer (NSCLC). Proceedings of the 18th EORTC-NCI-AACR Symposium on Molecular Targets and Cancer Therapeutics; 2006 Nov 7–10; Prague, Czech Republic.
7. Grunstein J, Roberts WG, Mathieu-Costello O, Hanahan D, Johnson RS. Tumor-derived expression of vascular endothelial growth factor is a critical factor in tumor expansion and vascular function. Cancer Res 1999;59:1592–8.
8. Ferrara N. Vascular endothelial growth factor: basic science and clinical progress. Endocr Rev 2004;25: 581–611.
9. Tischer E, Mitchell R, Hartman T, et al. The human gene for vascular endothelial growth factor. Multiple protein forms are encoded through alternative exon splicing. J Biol Chem 1991;266:11947–54.
10. Yamazaki Y, Morita T. Molecular and functional diversity of vascular endothelial growth factors. Mol Divers 2006;10:515–27.
11. Ferrara N, Gerber H-P, LeCouter J. The biology of VEGF and its receptors. Nat Med 2003;9:669–76.
12. Stimpfl M, Tong D, Fasching B, et al. Vascular endothelial growth factor splice variants and their prognostic value in breast and ovarian cancer. Clin Cancer Res 2002;8:2253–9.
13. Yu JL, Rak JW, Klement G, Kerbel RS. Vascular endothelial growth factor isoform expression as a determinant of blood vessel patterning in human melanoma xenografts. Cancer Res 2002;62:1838–46.
14. Carmeliet P, Ng Y-S, Nuyens D, et al. Impaired myocardial angiogenesis and ischemic cardiomyopathy in mice lacking the vascular endothelial growth factor isoforms VEGF164 VEGF188. Nat Med 1999;5:495–502.
15. Stalmans I, Ng YS, Rohan R, et al. Arteriolar and venular patterning in retinas of mice selectively expressing VEGF isoforms. J Clin Invest 2002;109:327–36.
16. Ruhrberg C, Gerhardt H, Golding M, et al. Spatially restricted patterning cues provided by heparin-binding VEGF-A control blood vessel branching morphogenesis. Genes Dev 2002;16:2684–98.
17. Grunstein J, Masbad JJ, Hickey R, Giordano F, Johnson RS. Isoforms of vascular endothelial growth factor act in a coordinate fashion to recruit and expand tumor vasculature. Mol Cell Biol 2000;20:7282–91.
18. Vieira JM, Schwarz Q, Ruhrberg C. Selective requirements for NRP1 ligands during neurovascular patterning. Development 2007;134:1833–43.
19. Parada LF, Land H, Weinberg RA, Wolf D, Rotter V. Cooperation between gene encoding p53 tumour antigen and ras in cellular transformation. Nature 1984;312:649–51.
20. Greco O, Coralli C, Dachs GU, et al. Role of VEGF in tumour response to vascular disrupting agents. Microcirculation 2005;12:681.
21. Kanthou C, Greco O, Stratford A, et al. The tubulin-binding agent combretastatin A-4-phosphate arrests endothelial cells in mitosis and induces mitotic cell death. Am J Pathol 2004;165:1401–11.
22. Chalkley HW. Method for quantitative morphologic analysis of tissues. J Natl Cancer Inst 1943;4:47–53.
23. Tozer GM, Ameer-Beg SM, Baker J, et al. Intravital imaging of tumour vascular networks using multi-photon fluorescence microscopy. Adv Drug Deliv Rev 2005;57:135–52.
24. Unthank J, Lash J, Nixon J, Sidner R, Bohlen H. Evaluation of carbocyanine-labeled erythrocytes for microvascular measurements. Microvascular Res 1993; 45:193–210.
25. Kimura K, Braun RD, Ong ET, et al. Fluctuations in red cell flux in tumor microvessels can lead to transient hypoxia and reoxygenation in tumor parenchyma. Cancer Res 1996;56:5522–8.
26. Tozer GM, Prise VE, Wilson J, et al. Mechanisms associated with tumor vascular shut-down induced by combretastatin A-4 phosphate: intravital microscopy and measurement of vascular permeability. Cancer Res 2001;61:6413–22.
27. Barber PR, Vojnovic B, Ameer-Beg SM, Hodgkiss RJ, Tozer GM, Wilson J. Semi-automated software for the three-dimensional delineation of complex vascular networks. J Microsc 2003;211:54–62.
28. Reyes-Aldasoro CC, Wilson I, Prise VE, et al. Estimation of apparent tumor vascular permeability from multiphoton fluorescence microscopic images of P22 rat sarcomas *in vivo*. Microcirculation 2008;15: 65–79.
29. Theiler JP, Gisler G. A contiguity-enhanced k-means clustering algorithm for unsupervised multispectral image segmentation. Proceedings SPIE 1997;3159: 108–18.
30. Eckhart L, Ban J, Ballaun C, Weninger W, Tschachler E. Reverse transcription-polymerase chain reaction products of alternatively spliced mRNAs form DNA heteroduplexes and heteroduplex complexes. J Biol Chem 1999;274:2613–5.
31. Zhang HT, Scott PA, Morbidelli L, et al. The 121 amino acid isoform of vascular endothelial growth factor is more strongly tumorigenic than other splice variants *in vivo*. Br J Cancer 2000;83:63–8.
32. McColm JR, Geisen P, Hartnett ME. VEGF isoforms and their expression after a single episode of hypoxia or repeated fluctuations between hyperoxia and hypoxia: relevance to clinical ROP. Mol Vis 2004;10: 512–20.
33. Guo P, Xu L, Pan S, et al. Vascular endothelial growth factor isoforms display distinct activities in promoting tumor angiogenesis at different anatomic sites. Cancer Res 2001;61:8569–77.
34. Kusters B, de Waal RM, Wesseling P, et al. Differential effects of vascular endothelial growth factor A isoforms

in a mouse brain metastasis model of human melanoma. Cancer Res 2003;63:5408–13.
35. Oshika Y, Nakamura M, Tokunaga T, et al. Ribozyme approach to downregulate vascular endothelial growth factor (VEGF) 189 expression in non-small cell lung cancer (NSCLC). Eur J Cancer 2000;36:2390–6.
36. Tokunaga T, Abe Y, Tsuchida T, et al. Ribozyme mediated cleavage of cell-associated isoform of vascular endothelial growth factor inhibits liver metastasis of a pancreatic cancer cell line. Int J Oncol 2002;21:1027–32.
37. Benjamin LE, Hemo I, Keshet E. A plasticity window for blood vessel remodelling is defined by pericyte coverage of the preformed endothelial network and is regulated by PDGF-B and VEGF. Development 1998;125:1591–8.
38. Soker S, Takashima S, Miao HQ, Neufeld G, Klagsbrun M. Neuropilin-1 is expressed by endothelial and tumor cells as an isoform-specific receptor for vascular endothelial growth factor. Cell 1998;92:735–45.
39. Gitay-Goren H, Soker S, Vlodavsky I, Neufeld G. The binding of vascular endothelial growth factor to its receptors is dependent on cell surface-associated heparin-like molecules. J Biol Chem 1992;267:6093–8.
40. Lee S, Jilani SM, Nikolova GV, Carpizo D, Iruela-Arispe ML. Processing of VEGF-A by matrix metalloproteinases regulates bioavailability and vascular patterning in tumors. J Cell Biol 2005;169:681–91.
41. Hutchings H, Ortega N, Plouet J. Extracellular matrix-bound vascular endothelial growth factor promotes endothelial cell adhesion, migration, and survival through integrin ligation. FASEB J 2003;17:1520–2.
42. Chaplin DJ, Pettit GR, Hill SA. Anti-vascular approaches to solid tumour therapy: evaluation of combretastatin A4 phosphate. Anticancer Res 1999;19:189–96.
43. Shaked Y, Ciarrocchi A, Franco M, et al. Therapy-induced acute recruitment of circulating endothelial progenitor cells to tumors. Science 2006;313:1785–7.
44. Landuyt W, Verdoes O, Darius DO, et al. Vascular targeting of solid tumours: a major 'inverse' volume-response relationship following combretastatin A-4 phosphate treatment of rat rhabdomyosarcomas. Eur J Cancer 2000;36:1833–43.
45. Beauregard DA, Hill SA, Chaplin DJ, Brindle KM. The susceptibility of tumors to the antivascular drug combretastatin A4 phosphate correlates with vascular permeability. Cancer Res 2001;61:6811–5.
46. Tozer GM, Kanthou C, Parkins CS, Hill SA. The biology of the combretastatins as tumour vascular targeting agents. Int J Exp Pathol 2002;83:21–38.
47. Yuan A, Yu CJ, Kuo SH, et al. Vascular endothelial growth factor 189 mRNA isoform expression specifically correlates with tumor angiogenesis, patient survival, and postoperative relapse in non-small-cell lung cancer. J Clin Oncol 2001;19:432–41.
48. Nakamura M, Abe Y, Tokunaga T. Pathological significance of vascular endothelial growth factor A isoform expression in human cancer. Pathol Int 2002;52:331–9.
49. Cressey R, Wattananupong O, Lertprasertsuke N, Vinitketkumnuen U. Alteration of protein expression pattern of vascular endothelial growth factor (VEGF) from soluble to cell-associated isoform during tumourigenesis. BMC Cancer 2005;5:128.
50. Jacobsen J, Grankvist K, Rasmuson T, Ljungberg B. Different isoform patterns for vascular endothelial growth factor between clear cell and papillary renal cell carcinoma. BJU Int 2006;97:1102–8.